Eur. J. Mineral.
2007, **19**, 547–556
Published online August 2007

Exsolution microstructures in amphiboles from metabasalts of the Betic ophiolitic association (SE Spain)

MARIA DOLORES RUIZ CRUZ[1,*], ENCARNACION PUGA[2] and ANTONIO DÍAZ DE FEDERICO[2]

[1] Departamento de Química Inorgánica, Cristalografía y Mineralogía, Facultad de Ciencias, Universidad de Málaga, 29071 Málaga, Spain
*Corresponding author, e-mail: mdruiz@uma.es
[2] Instituto Andaluz de Ciencias de la Tierra (CSIC-UGRA), Facultad de Ciencias, Avda. Fuentenueva s.n., 18002 Granada, Spain

Abstract: Exsolution microstructures in a complex amphibole assemblage from metabasalts of the Betic Ophiolitic Association (SE Spain) have been studied using transmission and analytical electron microscopy (TEM, AEM). Three main types of amphibole were identified, filling veins and vesicles: brown amphibole, with mean composition of pargasite, originated during an early ocean-floor metamorphism, and two types of green amphiboles with compositions of edenite and actinolite-magnesiohornblende, respectively formed during a later orogenic metamorphic event. The exsolution in the brown amphibole include minute rutile and amphibole rods. The brown amphibole also contains numerous halite inclusions. Amphibole exsolutions, with compositions of magnesiohornblende and actinolite appear to have formed paired rutile+amphibole intergrowths. All the exsolution products appear oriented with respect to the lattice of the host amphibole. Green amphiboles do not contain either submicroscopic rutile or halite inclusions, but they show oriented lamellae of magnesiokatophorite, exsolved in the edenite. These thin lamellae (300 to 500 Å in thickness) are coherently intergrown with the host. The studied amphibole pairs evidence two types of miscibility gaps: the one gap between amphiboles of the calcic group (brown amphibole) and the other gap between amphiboles of the calcic and sodic-calcic groups (green amphibole).

Key-words: ocean-floor metamorphism, orogenic metamorphism, Betic Cordillera, amphiboles, miscibility gap, exsolution, TEM/AEM.

Introduction

The most commonly used classifications of the amphiboles (Leake, 1978; Hawthorne, 1981, 1983; Leake *et al.*, 1997) are based on wet or electron microprobe (EMPA) analyses. In both cases, the presence of submicroscopic inclusions is neglected, although some of the elements contained in the more frequently described inclusions (*e.g.* rutile, ilmenite or spinel) are important in amphibole classification. A similar problem is posed by the presence of submicroscopic amphibole exsolution lamellae, which can notably influence the bulk amphibole composition. As a consequence, considerable attention has been devoted to the identification and analysis of these exsolution microstructures by TEM/AEM in the past decades (*e.g.* Ghose, 1981 and references therein; Smelik & Veblen, 1991, 1992, 1994).

Multiple amphibole assemblages have been identified in a variety of metamorphic rocks. Robinson *et al.* (1982, and references therein) have shown that three- and four-amphibole assemblages, in many cases visible by optical microscopy, commonly contain orthoamphiboles (anthophyllite and gedrite) and clinoamphiboles, both magnesian and calcic. On the other hand, the TEM/AEM study of Smelik & Veblen (1989) revealed a five-amphibole assemblage consisting of glaucophane, cummingtonite, winchite, actinolite and hornblende, all coexisting in a single grain. In this work we describe a complex amphibole assemblage, identified in metabasalts from the Cóbdar village (Fig. 1), which form part of the Betic Ophiolitic Association (BOA), defined by Puga (1990).

These ophiolitic rocks are discontinuously exposed along about 250 km in the Mulhacén Complex (Fig. 1). The geochemical characterization of the multiple amphibole assemblage was carried out by Puga *et al.* (2002) by electron microprobe (EMPA) and petrologic analyses. Brown amphiboles filling veins and vesicles in metabasalts have been interpreted by these authors as formed during an ocean floor metamorphism contemporary or slightly later than the magmatic episode, which originated the BOA during the Jurassic (Puga *et al*., 2000, 2005). The brown amphibole appears altered to green amphibole, which replaces in variable extent the brown grains and forms the innermost parts of veins and vesicles (Fig. 2). Green amphibole has been interpreted as formed during the Alpine

DOI: 10.1127/0935-1221/2007/0019-1735
0935-1221/07/0019-1735 $ 4.50

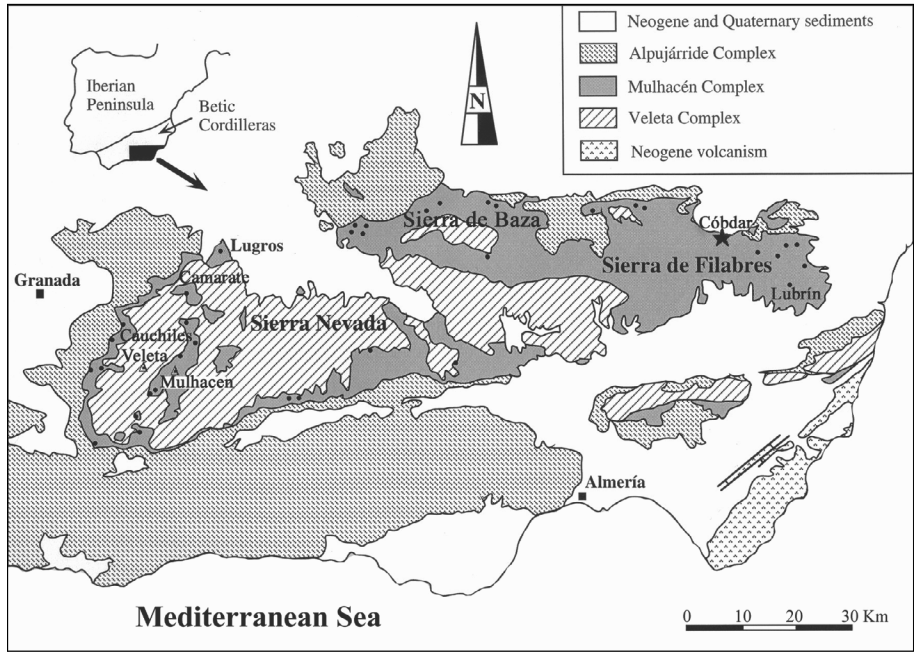

Fig. 1. Tectonic sketch map showing the relationships among the deepest metamorphic complexes forming the central-eastern sector of the Betic Cordillera. Filled circles on the Mulhacén Complex represent the location of the main outcrops of the Betic Ophiolitic Association exposed in Sierra Nevada and Sierra de Filabres according to Puga *et al.* (2002). The star indicates the Cóbdar village – the study area.

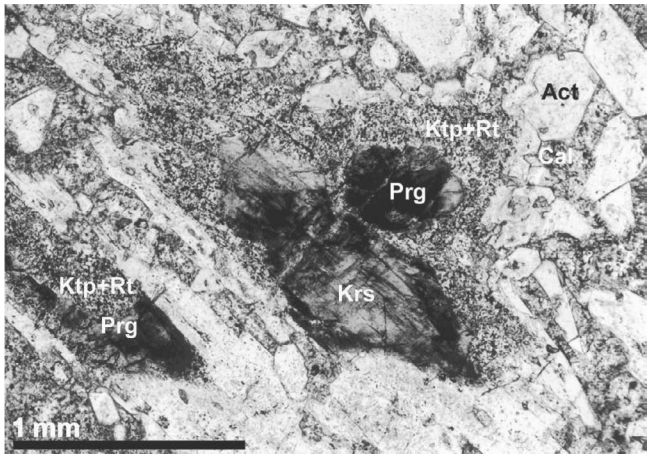

Fig. 2. Relics of brown amphibole (kaersutite and pargasite), partially altered to a thick corona of green amphibole (katophorite) with abundant microscopic grains of rutile and overgrown by a rim of clean green amphibole, which forms the innermost parts of the vein.

orogenic metamorphism, during the Oligocene to early Miocene times (Puga *et al*., 2000, 2005). The brown amphibole grains are commonly zoned, the mean composition of the core being kaersutite, which evolves in the external parts of the grains toward Ti-pargasite. The green amphiboles show a more variable composition, and two main groups, a calcic group (with actinolitic composition) and a sodic-calcic group (comprising barroisite, taramite and katophorite) have been identified, filling the innermost parts of veins and vesicles and overgrowing the brown amphibole grains. The formation of actinolitic amphibole is favored in calcite- or epidote-rich microdomains as shown in Fig. 2.

In the course of the TEM/AEM study of these amphiboles, a complex series of exsolution microstructures has been identified in coexisting amphiboles, which explains, at least in a part, the geochemical trends described by Puga *et al.* (2002). The exsolution includes amphibole lamellae, rutile, and rutile+amphibole rods. Although exsolved amphibole lamellae have been extensively studied, we are not aware of previously studied rods of amphibole and amphibole+rutile exsolution. The aim of this work is to study the mode of occurrence and composition of the several observed exsolutions and relate them with the metamorphic history of the metabasalts.

Experimental techniques

From the previous EMPA study, two basalt samples showing very different grade of alteration of the brown amphiboles into green amphiboles were selected for the TEM/AEM study. These samples were prepared by ion thinning selected areas of petrographic thin sections. Electron microscopy was performed at the CIC (Granada University) with a 200 kV Philips CM-20 transmission electron microscope fitted with a scanning transmission device and solid state detector for energy-dispersion analysis (EDX). Micro-analyses were carried out in STEM mode. Quantitative determinations used the thin-film approximation of Cliff & Lorimer (1975). Albite (Na), muscovite and annite (K), albite, spessartine and muscovite (Al), forsterite and annite (Mg and Fe), spessartine (Mn) and titanite (Ca and Ti) were used as standards. Calculation of

Table 1. End-term compositions for the amphiboles described in the text.

Calcic amphiboles	
Pargasite	$NaCa_2$ $[Mg_4Al]$ $[Si_6Al_2]$ $O_{22}(OH)_2$
Magnesiohastingsite	$NaCa_2$ $[Mg_4Fe^{3+}]$ $[Si_6Al_2]$ $O_{22}(OH)_2$
Edenite	$NaCa_2$ $[Mg_5]$ $[Si_7Al]$ $O_{22}(OH)_2$
Magnesiohornblende	$\square Ca_2$ $[Mg_4(Al,Fe^{3+})]$ $[Si_7Al]$ $O_{22}(OH)_2$
Tremolite	$\square Ca_2$ $[Mg_5]$ $[Si_8]$ $O_{22}(OH)_2$
Sodic-calcic amphiboles	
Magnesiotaramite	$Na(Ca,Na)$ $[Mg_3Al\ Fe^{3+}]$ $[Si_6Al_2]$ $O_{22}(OH)_2$
Magnesiokatophorite	$Na(Ca,Na)$ $[Mg_4\ (Al,Fe^{3+})]$ $[Si_7\ Al]$ $O_{22}\ (OH)_2$

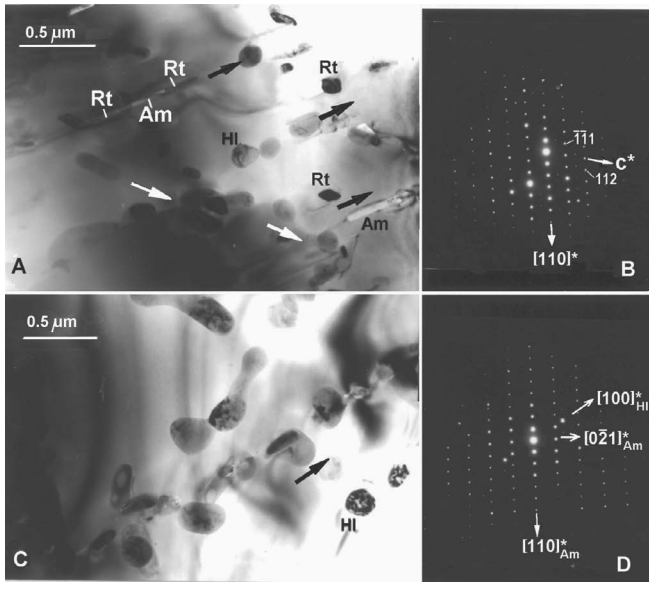

Fig. 3. A: Low magnification TEM images of inclusions in brown amphibole. Rutile (Rt), amphibole (Am) and halite (Hl) inclusions appear oriented following two main directions (arrows). The SAED pattern (B), viewed along [1$\bar{1}$0] of the host, only shows the amphibole reflections. C Halite inclusions-enriched area in the brown amphibole. The SAED pattern (D) obtained along [1$\bar{1}$ $\bar{2}$] of the amphibole, shows intense *h*00 reflections of halite.

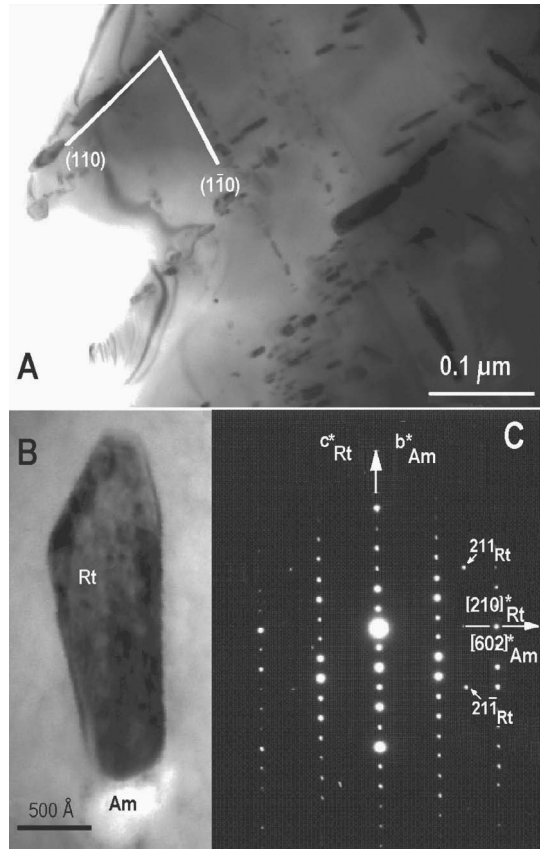

Fig. 4. A: Low magnification image showing the distribution of the rutile inclusions, following the symmetrically related (110) cleavage planes of the amphibole. B: Low magnification image of a rutile inclusion in which the elongation is parallel to its *c*-axis. C: The SAED pattern obtained over the rutile grain shown in B shows however, intense amphibole reflections and very weak rutile spots.

the amphibole formulae followed the method proposed by Schumacher (1997), and the nomenclature of amphiboles conforms to the recommendations of Leake *et al.* (1997). The formulae of the amphibole end-members cited in the paper have been summarized in Table 1. The abbreviations of minerals suggested by Kretz (1983) have been used in the text, tables and figures, with some additions indicated in the captions of the figures.

TEM-AEM study

Brown amphibole

Low-magnification TEM observation of the brown amphibole grains (or areas) reveals that they contain numerous differently shaped inclusions, which include three main types (Fig. 3, 4): 1) subhedral, elongated rutile inclusions, with dark contrast in the images; 2) elongate, light amphibole inclusions; and 3) rounded and mottled halite inclusions. Moreover, composite inclusions formed by rutile and amphibole are also frequent. Commonly, rutile and amphibole crystals share the longest dimension of the prisms

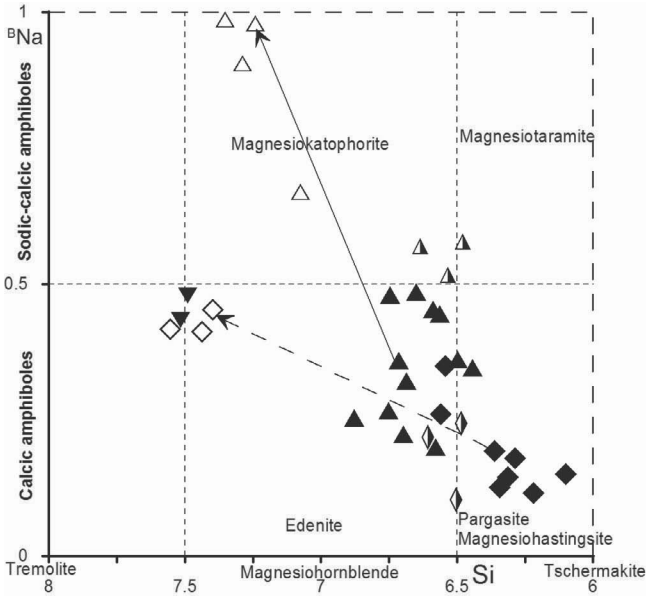

Fig. 5. Classification of the studied amphiboles in the diagram of Leake et al. (1997). Meaning of the symbols: full diamond = brown amphibole; open diamond = exsolutions in the brown amphibole, half-open diamond = mixed analyses between brown amphibole and their exsolutions; filled triangle = edenitic green amphibole; open triangle = exsolved lamellae in the edenitic amphibole: half-open triangle = mixed analyses between green edenite and their exsolutions; inverted triangle = actinolitic green amphibole. Dashed-line and continuous-line arrows represent, respectively, brown and green coexisting pairs of exsolutions and hosting amphiboles.

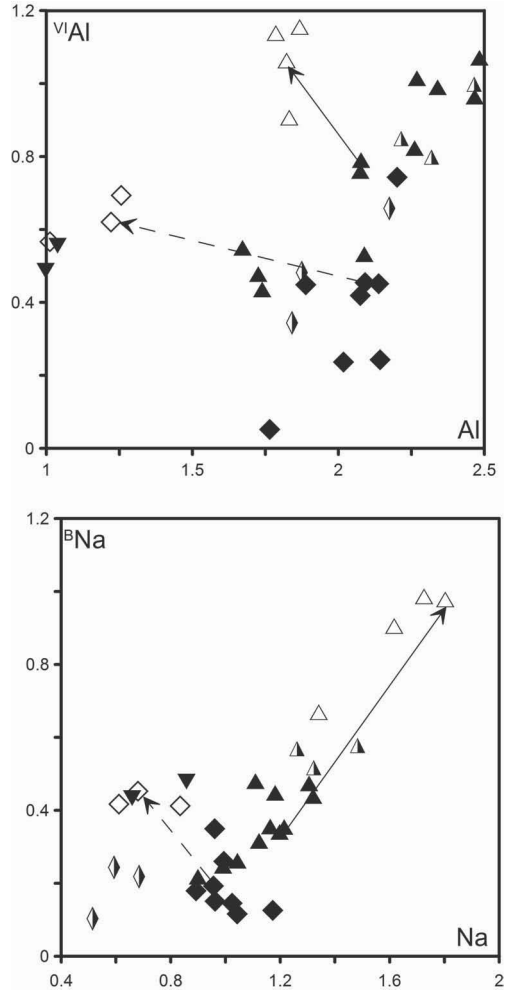

Fig. 6. Plot of the same amphiboles represented in Fig. 5 in the ^{VI}Al *vs.* Al (A) and ^{B}Na vs. Na (B) diagrams.

in elongate composite precipitates. Nevertheless, in some cases, long inclusions show an alternation of amphibole and rutile, along the elongation direction (Fig. 3A). Some areas of the brown amphibole (*e.g.* Fig. 3A) show a similar content of rutile + amphibole and halite inclusions; other areas (*e.g.* Fig. 3C) mainly contain halite inclusions; whereas, in some other areas (*e.g.* Fig. 4A) halite inclusions are very scarce. In spite of their irregular distribution, an approximate estimation of their content in several areas indicates that the mean values range from 3 % to ≈15 % in volume. These values are in agreement with the Cl content determined by electron microprobe in the brown amphiboles (Puga *et al.,* 2002).

All the AEM data of brown amphibole that were obtained in inclusions-free areas correspond to the calcic amphibole group and show a pargasite composition, with variations toward magnesiohastingsite or edenite (Fig. 5). These amphiboles are characterized by lower Si and ^{B}Na contents, higher Ti content, and intermediate Al and Na contents by respect the other amphibole filling the same veins (Table 2, Fig. 5 and 6). In addition, the Cl content is below the detection level.

Halite inclusions normally appear as arrays of particles with a common orientation relative to the host amphibole, perpendicular either to $(\bar{1}\,\bar{1}\,1)$ or to (112) of amphibole (Fig. 3A and B). Halite shows intense 100 reflections in the SAED pattern (Fig. 3D).

Rutile inclusions do not display a fixed orientation relative to the host amphibole, although some orientations dominate. Figure 4A reveals that the rutile inclusions lie on the symmetrically related (110) cleavage planes of the amphibole, where they follow the [110] direction as well as the directions perpendicular to $(\bar{1}\,\bar{1}\,1)$ and (112) of the amphibole (Fig. 3A, B). Figure 4B shows a rutile inclusion in which the elongation is parallel to the *c*-axis of this crystal. Despite the very weak reflections of rutile, the SAED pattern (Fig. 4C) permits the establishment of the following topotactic relationships with amphibole: $(010)_{Am}//(001)_{Rt}$ and $(001)_{Am}//(010)_{Rt}$, in such a way that the oxygens packing is parallel in both phases. This orientation has been previously described by Mongkoltip & Ashworth (1983). All these geometrical relationships indicate that rutile inclusions formed through an exsolution process.

Both halite and rutile inclusions are easily identified using the AEM data but amphibole rods, which appear as single crystals or associated to rutile grains, are minute and the obtaining of accurate analyses is very difficult. The high-resolution images indicate that these inclusions maintain the structure and the orientation of the host amphibole,

Table 2. Selected AEM data on brown amphiboles (B) and inclusions (I).

	B-1	B-2	B-3	B-4	B-5	B-6	B-7	B-9	I-4	I-5	I-6
	Fig. 3A	Fig. 3B	Fig. 4	Fig. 7	Fig. 10	Fig. 10	Fig. 10	NS	Fig. 7	Fig. 7	NS
Formula to 23 (O)											
Si	6.56	6.22	6.54	6.36	6.31	6.34	6.10	6.29	7.40	7.44	7.55
^{IV}Al	1.44	1.78	1.46	1.64	1.69	1.66	1.90	1.71	0.60	0.56	0.45
^{VI}A	0.45	0.24	0.74	0.45	0.45	0.42	0.24	0.05	0.62	0.69	0.57
Ti	0.12	0.27	0.24	0.21	0.12	0.16	0.32	0.44	0.04	0.11	0.12
Fe^{3+}	0.28	0.20	0.00	0.19	0.26	0.00	0.36	0.20	0.13	0.00	0.00
Fe^{2+}	0.95	1.13	1.10	1.05	1.02	1.29	0.88	1.08	0.83	0.89	0.91
Mg	3.28	3.23	2.91	3.15	3.22	3.13	3.30	3.29	3.42	3.24	3.38
Ca	1.66	1.83	1.65	1.75	1.78	1.87	1.75	1.76	1.51	1.59	1.58
^{B}Na	0.26	0.12	0.35	0.19	0.15	0.13	0.15	0.18	0.45	0.41	0.42
^{A}Na	0.73	0.93	0.61	0.76	0.88	1.05	0.81	0.71	0.23	0.42	0.19
K	0.00	0.00	0.00	0.00	0.00	0.00	0.00	0.05	0.00	0.00	0.00
Σ cat	15.73	15.95	15.60	15.75	15.88	16.05	15.81	15.76	15.23	15.35	15.17
Cl	0.00	0.00	0.00	0.00	0.00	0.00	0.00	0.00	0.00	0.00	0.00
	(Ed)	(TiPrg)	(Ed)	(Prg)	(Prg)	(Prg)	(TiMgHst)	(TiMgHst)	(MgHb)	(MgHb)	(Act)

Symbols used: NS: Not shown in the TEM images; Ed: Edenite; Prg: Pargasite; TiPrg: Titanian pargasite; TiMgHst: Titanian magnesiohastingsite; MgHb: MagnesiohHornblende; Act: Actinolite

although splitting was not observed, probably due to the very small size of the amphibole precipitates. From the several analyses obtained from the rods, only three, acquired on the largest inclusions, appear to be uncontaminated. These indicated magnesiohornblende and actinolite compositions (Fig. 5). These analyses showed Al and Na contents lower than the corresponding host amphibole, as shown in Fig. 6. These data indicate partitioning of Al between the two types of amphibole. In general, the hornblende precipitates have higher ^{B}Na, and lower Ti and Na than the host pargasite (Table 2, Fig. 5 and 6, and spectra inset in Fig. 7).

In contrast to the exsolution lamellae frequently observed in amphiboles (Ghose, 1981), which show two large dimensions, these amphibole precipitates appear as short prisms or rods (in the order of 0.1–0.5 μm in length) with two short dimensions (ranging from 50 to 500 Å). Thus, it is only possible the determination of the orientation of the direction of elongation. This orientation is frequently coincident with that of the rutile precipitates (Fig. 3A and 4A), with $c^*_{Rt}//b^*_{Am}$. Nevertheless, in the case of Fig. 7, the amphibole precipitate shows elongation nearly parallel to the $(\bar{2}\bar{2}1)$ plane.

The location of the exsolved rutile+amphibole crystals, mainly following the (110) cleavage planes of the amphibole suggests an inhomogeneous mechanism of nucleation for these inclusions.

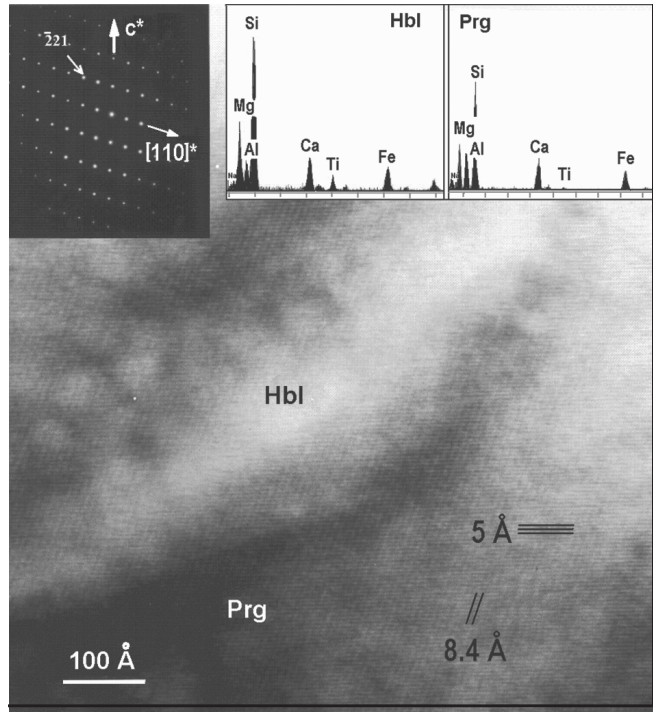

Fig. 7. Lattice-fringe image of a magnesiohornblende inclusion (Hbl) in pargasite (Prg). The image shows the coincidence of the two lattices. The elongation of the inclusion is perpendicular to the $(\bar{2}\bar{2}1)$ planes of the host, as indicated by the SAED pattern. Inset: EDX spectra for the two amphiboles.

Green amphibole

TEM observation of the green amphiboles reveals important differences between these and the coexisting relics of brown amphibole: on the one hand, they display numerous crystalline defects, such as arrays of regularly spaced dislocations. In addition, green amphiboles do not contain either rutile or halite inclusions. When examined by TEM,

Table 3. Selected AEM data on green amphiboles (G = Main population 1. T = Minor population) and exsolved lamellae in the main population (L).

	G-1 Fig. 8A	G-2 Fig. 8B	G-3 Fig. 8B	G-4 Fig. 8B	G-5 Fig. 9	G-6 Fig. 9	G-7 NS	G-8 NS	G-9 NS	G-11 NS	G-15 NS	T-1 NS	T-2 NS	L-1 Fig. 8B	L-2 Fig. 9	L-3 NS	L-4 NS
Formula to 23 (O)																	
Si	6.75	6.70	6.88	6.59	6.69	6.71	6.75	6.65	6.56	6.50	6.44	7.49	7.52	7.08	7.24	7.35	7.29
^{IV}Al	1.25	1.30	1.12	1.41	1.31	1.29	1.25	1.35	1.44	1.50	1.56	0.51	0.48	0.92	0.76	0.65	0.71
^{VI}Al	0.48	0.44	0.55	1.07	0.76	0.79	1.01	0.99	0.82	0.96	0.53	0.49	0.56	0.91	1.06	1.14	1.16
Ti	0.01	0.00	0.04	0.04	0.00	0.02	0.00	0.05	0.04	0.04	0.02	0.00	0.00	0.00	0.00	0.00	0.00
Fe^{3+}	0.15	0.32	0.00	0.00	0.00	0.00	0.00	0.00	0.00	0.00	0.47	0.12	0.14	0.00	0.00	0.00	0.00
Fe^{2+}	0.85	0.68	1.01	1.04	1.25	1.29	1.33	1.41	1.17	1.29	0.83	0.68	0.62	1.18	1.02	1.05	1.06
Mg	3.55	3.66	3.38	2.83	2.96	2.85	2.61	2.55	2.96	2.67	3.29	3.74	3.72	2.90	2.88	2.76	2.73
Ca	1.70	1.69	1.75	1.55	1.68	1.65	1.53	1.52	1.56	1.64	1.52	1.49	1.53	1.33	1.02	1.01	1.09
^{B}Na	0.26	0.22	0.25	0.45	0.32	0.35	0.47	0.48	0.44	0.36	0.34	0.48	0.43	0.67	0.98	0.99	0.91
^{A}Na	0.78	0.68	0.74	0.73	0.81	0.86	0.83	0.63	0.88	0.81	0.86	0.38	0.22	0.67	0.82	0.74	0.71
K	0.08	0.08	0.08	0.06	0.23	0.20	0.16	0.11	0.12	0.20	0.00	0.00	0.00	0.07	0.02	0.03	0.03
Σcat	15.86	15.77	15.80	15.76	16.01	16.01	15.94	15.74	15.99	15.97	15.86	15.38	15.22	15.73	15.80	15.72	15.69
Cl	0.30	0.00	0.00	0.50	0.50	0.50	0.30	0.60	0.40	0.40	0.30	0.00	0.00	0.20	0.20	0.30	0.10
	(Ed)	(Ed)	(Ed)	(AlEd)	(Ed)	(Ed)	(AlEd)	(Ed)	(Ed)	(Prg)	(Prg)	(MgHb)	(Act)	(MgKtp)	(AlMgKtp)	(AlMgKtp)	(AlMgKtp)

Symbols used: NS: Not shown in the TEM images; Ed: Edenite; AlEd: Aluminoedenite; Prg: Pargasite; MgHb: Magnesiohornblende; Act: Actinolite; MgKtp Magnesiokatophorite; AlMgKtp: Aluminiomagnesiokatophorite.

Fig. 8. TEM images showing the lamellae exsolved in the green amphibole. A: Curved interfaces. B: Straight interfaces parallel to (110).

exsolution microstructures, not evident from optical and EMPA examination, were identified in these amphiboles (Fig. 8), being similar to that described by Ghose (1981) and Smelik & Veblen (1991, 1992, 1994) among others.

Analytical electron microscopy (AEM) data on green amphibole indicate, in agreement with the EMPA analyses, two populations of green amphibole. One of these populations (main population) is notably more abundant in the samples studied by TEM, and shows a mean composition of edenite and minor pargasite; whereas, the other (minor population) is actinolite-magnesiohornblende (Table 3, Fig. 5). The spectra of the main population show some K and Cl contents and they do not contain halite inclusions as the brown amphiboles do.

AEM data of the exsolved lamellae indicate a more siliceous composition. Some of the analyses, obtained with a very fine probe, are shown in Table 3, and show a mean composition of magnesiokatophorite (Fig. 5). Nevertheless, since the lamellae are quite narrow (100−300 Å), the X-ray spectra frequently contain some contributions from the surrounding host, given mixed analyses, some of which have also been represented in Fig. 5 and 6. The compositional differences between the lamellae and the green amphibole mainly consists in a Ti and ^{IV}Al decrease and a Na, ^{B}Na and ^{VI}Al increase (Table 3 and Fig. 5 and 6).

Low magnification and Lattice fringe images indicate that the exsolved lamellae mainly occur in one orientation, the interfaces being coherent and somewhat curved (Fig. 8), probably reflecting a close similarity of the unit-cell parameters of the two amphiboles (Smelik & Veblen, 1992). Both concentration and coarseness of the lamellae vary from grain to grain and even within single grains. Generally, an increase of the lamellae concentration is observed at increasing distances of the brown amphibole relicts, *i.e.* towards the periphery of the green amphibole grains. One anomalously coarse lamellae approaching 800 Å in thickness is shown in Fig. 9. This lamella allowed a relatively accurate determination of the orientation. Figure 9 is a view down the [$\bar{1}$10] zone of this area and shows the 8.4-Å characteristic periodicity of the (110) planes. Although the reflections of the lamella are not discernible in the SAED pattern, the lattice fringe image reveals that the lamella is

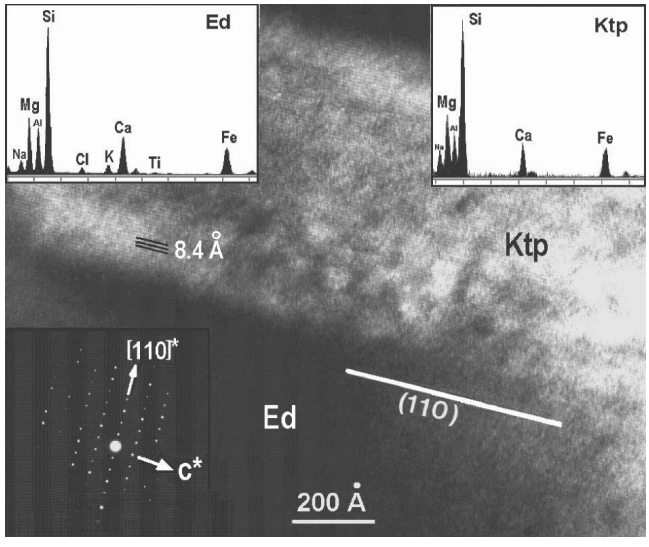

Fig. 9. Lattice fringe image of a thick magnesiokatophorite lamella exsolved in edenite. The lamella, richer in Na, appears more damaged by the electron beam. The image is viewed down [$\bar{1}$10]. The lattice-fringe image reveals that the magnesiokatophorite lamella is oriented paralel to the (110) planes. Inset: EDX spectra of the two amphiboles.

parallel to the (110) plane. Differences in composition between host and lamella are shown in Fig. 9 (spectra inset).

The minor population of green amphibole, formed by actinolite and magnesiohornblende, is scarcely represented in the samples studied by TEM. In fact, these types of amphiboles have only been identified associated to clinozoisite-rich micro-domains, forming narrow crystals intimately intergrown with the clinozoisite. The amphiboles of this minor population show a composition straddling actinolite and magnesiohornblende fields, characterized by notably higher Si contents and Mg/(Fe+Mg) ratios, and lower Ti and Al that those forming the main green amphibole population (Table 3, Fig. 5 and 6). In addition, they do not contain detectable Cl or K, in opposition to the main green amphibole population and they are chemically more similar to the amphibole rods exsolved in the brown amphibole group.

Discussion

The only evidence of exsolution from optical examination of these amphiboles was the presence of abundant rutile needles included in the green amphibole areas formed from the brown amphibole (Fig. 2). Nevertheless, TEM examination shows the presence of several types of submicroscopic particles and lamellae, which represent additional distinction criteria between green and brown amphiboles. Two main aspects of the described amphiboles merit a more detailed discussion: 1) the chemical evolution of the amphiboles through the several metamorphic stages; and 2) the miscibility gaps observed between the two pairs of amphiboles.

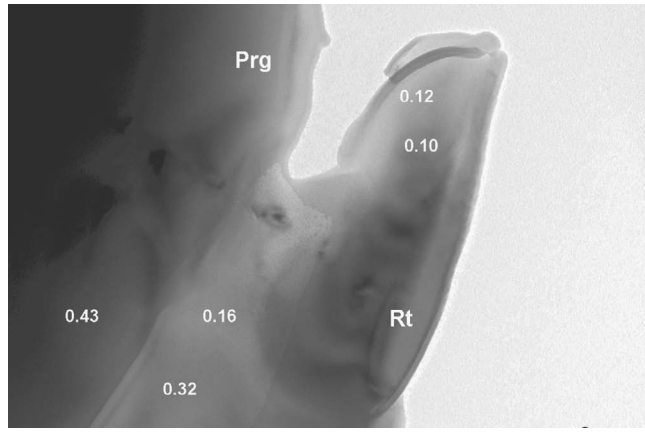

Fig. 10. Ti content (apfu) in the analyses of the brown amphibole host, obtained at variable distance of the rutile (Rt) inclusion.

Chemical evolution of the amphiboles

Chemical characterization of the brown and green amphiboles based on EMPA data was discussed in detail by Puga *et al.* (2002). Here we summarize some of the chemical characteristics of the AEM study, which agree in some cases with the EMPA results, and in other cases complete them.

Figures 5 and 6 show some chemical characteristics for the different types of amphibole analyzed by AEM, which confirm the differences in T and P genetic conditions previously deduced from the EMPA data. Thus, brown amphiboles show higher Ti and ^{IV}Al contents and lower values of ^{B}Na and ^{VI}Al than the green amphiboles. These chemical differences reflect higher T and lower P for the brown amphiboles than for the green amphiboles (Raase, 1974; Robinson *et al.,* 1982), and led to Puga *et al.* (2002) to deduce different stages of genesis for the two main amphibole groups. Brown amphibole paragenesis would be formed during the ocean-floor metamorphic stage (dated as late Jurassic); whereas, green amphibole paragenesis was considered as developed during a mesoalpine orogenic metamorphic event, which affected the Betic ophiolites during the Oligocene, generating P-T conditions corresponding to the Ab-Ep amphibolite facies (Puga *et al*., 2000, 2005).

The TEM study has led us to identify other two types of amphiboles, exsolved into the brown and the green amphiboles, whose chemical characteristics are also plotted in Fig. 5 and 6. Chemical variations between exsolved amphiboles and hosts have been indicated by two arrows jointing two representative pairs of exsolved and host crystals. These differences must be interpreted as a function of both the genetic conditions and the chemical composition of the submicroscopic microdomains in which the exsolution took place. In the case of the brown amphiboles, the Ti contents appear to be related with the distance between the analyzed area and the rutile precipitates; thus, point analyses obtained at increasing distances of the rutile inclusions show increasing amounts of Ti (Fig. 10). In the case of the green amphiboles, in spite of their low Ti contents, a Ti partitioning between host and exsolved lamellae was

observed, in such a way that the Ti content is below the detection level in the exsolved lamellae.

Another notable difference between brown and green amphiboles concerns to their Cl content. The AEM analyses show no Cl in the brown amphiboles (Fig. 7, inset); whereas, this element was present in the EMPA analyses of these amphiboles (Fig. 8 in Puga *et al*., 2002). This clearly indicates that the Cl content determined by EMPA in the same samples must correspond to the halite inclusions present in the brown amphiboles (Fig. 3). This saline phase was also identified forming inclusions in olivine from gabbro of the same ophiolitic outcrop than the metabasalts described here, and were interpreted by Puga et al. (1999) as formed by infiltration of sea water on the igneous paragenesis during the ocean-floor metamorphic stage. On the other hand, the Cl content is very different in the two populations of green amphiboles: The main population, that replaces brown amphibole grains, show variable Cl contents whereas the minor population, neoformed together with epidote or calcite, does not contain Cl. The incorporation of the saline inclusions contained in the preexisting brown amphiboles, in the structure of the green amphiboles replacing them, would explain the Na and Cl contents characterizing the main green amphibole population. A similar behavior is observed in relation with the K content, which is only present in the edenitic green amphiboles of the main population (Table 3, inset in Fig. 9). In spite that several factors can control the Cl substitution in the OH side of the amphiboles (Morrison, 1991; Enami et al., 1992), our results suggest that the chlorine content is mainly favored by the entry of large K cations in the amphibole structure, as shown by Volfinger *et al.* (1985).

In spite of their different composition, the two populations of green amphibole show, in accordance with the EMPA data, a common trend of increase in ^{B}Na and ^{VI}Al by respect the brown amphiboles (Fig. 6), which indicates a pressure increase, corresponding to the change from the oceanic-floor environment to that of the orogenic metamorphism. Presence of parallel intergrowths actinolite+clinozoisite confirms that the green amphibole growth was coetaneous with clinozoisite formation, during the orogenic metamorphism in Ab-Ep amphibolite facies conditions.

The amphibole lamellae exsolved into the green amphibole present the highest Na and ^{B}Na content and also the highest ^{VI}Al. These data indicate that they originated near the highest pressure conditions attained during the mesoalpine orogenic metamorphic event, whose climax was calculated by Puga *et al.* (2002) for about 7−8 kbar and 500−550 °C, using the amphibole-plagioclase geothermometer of Holland & Blundy (1994).

The amphibole rods exsolved into the brown amphibole show Na and Al contents lower than the lamellae exsolved in the green amphibole, but similar to the minor population of green amphiboles, indicating that they also grew during the increasing pressure conditions related to the prograde stage of the orogenic metamorphism. The relative P and T conditions for the different types of amphiboles described here may be deduced from Fig. 11, because they are function of their ^{B}Na and ^{IV}Al values, respectively, according

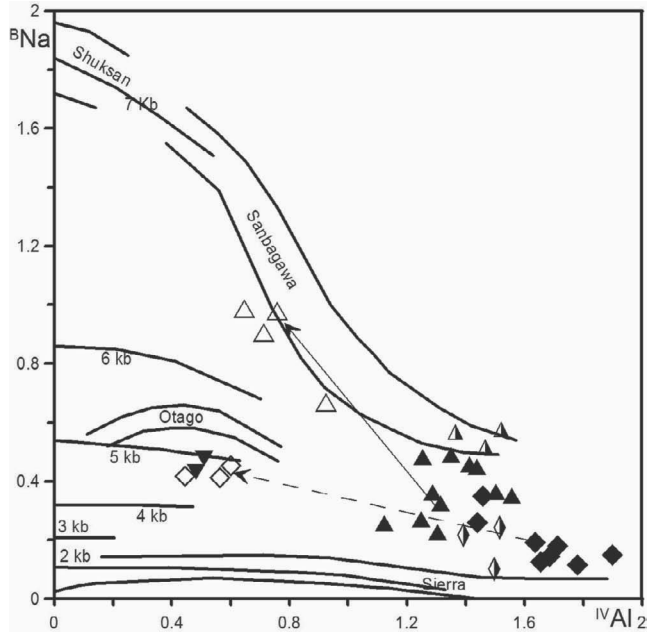

Fig. 11. Plot of the studied amphiboles on the Brown's diagram (1977) that shows a tentative relationship between pressure (^{B}Na) and temperature (^{IV}Al). Meaning of symbols and arrows as in Fig. 5.

to Brown (1977). These thermobarometric estimations are only strictly applicable to microdomains with similar Al and Na contents.

Exsolution of rutile could be originated during cooling of hosting amphiboles (Mongkoltip & Ashworth, 1983). Nevertheless, in our case, the pressure genetic conditions of the amphiboles exsolved together with the rutile rods are, according to their ^{B}Na values, clearly higher than those corresponding to the cooling process of the hosting brown amphibole, which formed in an oceanic-floor metamorphic environment. Thus, it is more probable that the rod exsolutions took place during the prograde stage of the orogenic metamorphism, at similar conditions to those originating the minor population of green amphibole in these metabasalts. Moreover exsolution of sodic-calcic amphibole lamellae in the main green amphibole population appears to have taken place near the highest P conditions of the mesoalpine metamorphism.

The miscibility gaps

As indicated by Robinson *et al.* (1982), the presence of amphibole lamellae in another amphibole is one of the surest and soundest pieces of evidence for a crystal-chemically-controlled miscibility gap in coexisting amphiboles. Thus, Smelik *et al.* (1991) presented solid evidence from submicroscopic exsolution, for the existence of an actinolite-hornblende miscibility gap.

Exsolution microstructures involving calcic and ferromagnesian amphiboles were revised by Ghose (1981) and Robinson *et al.* (1982). More recent contributions relative

to the cummingtonite-hornblende pair are those of Klein et al. (1996, 1997). Exsolution involving alkali and ferromagnesian amphiboles have been reported by Klein (1966, 1968), Robinson *et al*. (1971), Ghose *et al.* (1974), Shau *et al*. (1993); Smelik & Veblen (1989, 1991). Exsolution involving alkali and calcic amphibole has been reported by Smelik & Veblen (1989, 1992, 1994). On the other hand, exsolution within the calcic amphibole series (actinolite-hornblende) was described in detail by Smelik *et al.* (1991).

The compositional variation in amphibole is well described in terms of exchange vectors (Thompson, 1982a, b). In the case of exsolutions, the immiscible pairs provide at least two points in composition space, which permit the derivation of the vectors. We have applied the derivation method of Zingg (1996) for estimating the main vectors defining the miscibility gaps in the pargasite-actinolite and edenite-magnesiokatophorite pairs described in this work.

In the case of immiscibility in calcic amphiboles, three main vectors are generally the most important for defining the miscibility gap: the edenitic ($NaAl\square^{IV}_{-1}Si_{-1}$), the tschermak's ($^{VI}Al^{IV}AlMg_{-1}Si_{-1}$), and the $Fe^{2+}Mg_{-1}$ vectors (Robinson *et al*., 1982). From the derivation of the additive component (AC) and the target component (TC), we have deduced the following bulk vector for the brown amphibole exsolution:

$$Na_{0.60}Ca_{0.33}Fe^{2+}_{0.17}Fe^{3+}_{0.33}Ti^{IV}_{0.28}Al_{2.0}Mg^{VI}_{-0.30}Al_{-0.50}Si_{-2.0}$$

From this bulk vector, several substitutions appear to be important: The notable increase on ^{A}Na (decrease of the vacancies number) in host relative to the exsolved rods suggests that the edenitic vector ($Na^{IV}Al\square^{IV}_{-1}Si_{-1}$) is the most significant in this pair. Presence of Fe^{3+} suggests that the ferritschermakite exchange $Fe^{3+IV}AlMg_{-1}Si_{-1}$ has some contribution. On the contrary, from the sign of the ^{VI}Al and ^{IV}Al components it is evident that the tschermakitic vector does not participate in the exchange. This fact prevents the direct application of the Zingg method and requires numerous calculations, assuming several combinations of possible vectors. The better results were obtained starting from the derivation of the edenitic vector, directly from the vacancies. This leads to a value of 0.91 (size of the vector) for this exchange. The size of the plagioclase vector $Ca^{IV}AlNa_{-1}Si_{-1}$ (0.40) was derived from Ca, and that of the ferritschermakite vector (0.33), from Fe^{3+}. Finally, the Ti-tschermakite vector $^{IV}Al_2TiSi_{-2}Al^{VI}_{-1}$ (0.28) fits the final values better than the simpler $TiSi_{-1}$ vector.

Thus, exsolution observed in the brown amphibole is an evidence for the existence of a pargasite-actinolite miscibility gap. It seems that exsolution of actinolite was mainly controlled by the chemical rearrangement of the host amphibole in the contact with the rutile exsolutions. Indeed, loss of Ti from the Ti-rich amphiboles shown by Puga *et al.* (2002) would originate an increase of both Si and ^{B}Na contents and a parallel decrease of the A-site occupancy, which would originate actinolite-magnesiohornblende from pargasite.

In the case of the green amphiboles (edenite-magnesiokatophorite pair), the bulk vector deduced from the A and T components is:

$$Ca_{1.10}(Fe^{2+} + Mg)_{0.40}Fe^{3+}_{0.22}Ti^{IV}_{0.06}Al_{1.50}$$
$$(Na + K)^{VI}_{-1.0}Al_{-0.60}Si_{-1.50}$$

As in the case of the brown amphiboles, the opposite signs of ^{VI}Al and ^{IV}Al suggests lack of tschermakite substitution. Although $Mg+Fe^{2+}$ correlates with Si, no correlation between Mg and the other cations was found, and we used the $Mg+Fe^{2+}$ component for deriving the vectors. The most evident exchange is $Ca(Na+K)_{-2}$. This exchange can be accounted for different vectors: the glaucophane $CaMgNa^{VI}_{-1}Al_{-1}$ and the riebeckite $CaMgNa^{VI}_{-1}Fe^{3+}_{-1}$ vectors, which are the most significant in the case of the miscibility gap between sodic and calcic amphiboles (Smelik & Veblen, 1992), and the plagioclase $Ca^{IV}AlNa_{-1}Si_{-1}$ vector. It is evident from the bulk vector that the riebeckite substitution does not participate in this gap. The contribution of the other two vectors is difficult to estimate; the better results were obtained for 0.60 glaucophane and 0.40 plagioclase. The $Fe^{3+IV}AlMg_{-1}Si_{-1}$ vector is suggested by the increase of Fe^{3+} in the calcic term and also can be derived directly (0.22). After these estimations, residual Mg, and ^{VI}Al and Si strongly suggests the contribution of minor substitutions such as $\square Mg^{IV}_2Al^{VI}Al_{-1}Si_{-1}$ and $\square_{0.33}Ti^{VI}Al_{-1.33}$. It is also possible that some other coupled substitutions involving the $O(OH)_{-1}$ exchange (Poop & Bryndzia, 1992) be also important in this miscibility gap.

Conclusions

The results from this study indicate that the amphiboles filling veins and vesicles in metabasalts from the BOA (Betic Cordillera, Spain) record a complex history of exsolution. Primary brown amphibole, originated during the ocean-floor metamorphic stage that followed the magmatic process, was rich in Ti and contained submicroscopic halite inclusions. This amphibole type remained in metastable state from the Late Jurassic up to attain the prograde stage of the mesoalpine orogenic event, during which a part of the Ti was exsolved forming submicroscopic rutile rods. This exsolution stage also formed rutile+actinolite precipitates through a mechanism of inhomogeneous nucleation in the host brown parental amphibole.

The second episode of exsolution formed lamellae of magnesiokatophorite irregularly distributed in the green calcic amphibole. This stage of exsolution must have occurred at temperatures and pressure near of 550 °C and 8 kbar, determined by Puga *et al.* (2002) as corresponding to the metamorphic climax conditions of the mesoalpine metamorphic event in the Cóbdar Ophiolites.

Acknowledgements: The authors are grateful to J.C. Schumacher and M. Enami, whose corrections and suggestions notably improved the manuscript and to M.M. Abad for help in obtaining the TEM/AEM data. Financial support from the Project BTE 2003-09808 (Ministerio de Educación y Ciencia) and from the RNM 333 Research Group (Junta de Andalucía) is acknowledged.

References

Brown, E.H. (1977): The crossite content of Ca-amphiboles as a guide to pressure of metamorphism. *J. Petrol.*, **18**, 53-72.

Cliff, G. & Lorimer, G.W. (1975): The quantitative analysis of thin specimens. *J. Microscopy,* **103**, 203-207.

Enami, M., Liou, J.G., Bird, D.K. (1992): Cl-bearing amphibole in the Salton Sea geothermal system, California. *Can. Mineral*., **30**, 1077-1092.

Ghose, S. (1981): Subsolidus reactions and microstructures in amphiboles. *Rev. Mineral*., **9A.** 325-372.

Ghose, S., Forbes, W.C., Phakey, P.P. (1974): Unmixing of an alkali amphibole (tirodite) into magnesio-richterite and magnesio-riebeckite. *Indian J. Earth Science*, **1**, 37-42.

Hawthorne, F.C. (1981): Crystal chemistry of the amphiboles. *Rev. Mineral*., **9A**, 1-102.

– (1983): The crystal chemistry of the amphiboles. *Can. Mineral*., **21**, 173-480.

Holland, T. & Blundy, J. (1994): Non-ideal interaction in calcic amphiboles and their bearing on amphibole-plagioclase thermometry. *Contrib. Mineral. Petrol*., **116**, 433-447.

Klein, C. (1966): Mineralogy and petrology of metamorphosed Wabush Iron Formation, south-western Labrador. *J. Petrol*., **7**, 246-305.

– (1968): Coexisting amphiboles. *J. Petrol*., **9**, 281-330.

Klein, U., Schumacher, J.C., Cank, M. (1996): Mutual exsolution in hornblende and cummingtonite: Compositions, lamellae orientations, and exsolution temperatures. *Am. Mineral*., **81**, 928-939.

Klein, U., Sharp, T.G., Schumacher, J.C. (1997): Analytical electron microscopy of nanometer-scale hornblende lamellae: Low-temperature exsolution in cummingtonite. *Am. Mineral*., **82**, 1079-1090.

Kretz, R. (1983): Symbols for rock-forming minerals. *Am. Mineral*., **68**, 277-279.

Leake, B.E. (1978): Nomenclature of amphiboles. *Am. Mineral*., **63**, 1023-1053.

Leake, B.E., Woolley, A.R., Arps, C.E.S., Birch, W.D., Gilbert, M.C., Grice, J.D., Hawthorne, F.C., Kato, A., Kisch, H.J., Krivovichev, V.G., Linthout, K., Laird, J., Mandarino, J.A., Maresch, W.V., Nickel, E.H., Rock, N.M.S., Schumacher, J.C., Smith, D.C., Stephenson, N.C.N., Ungaretti, L., Whitaker, E.J.W., Guo, Y. (1997): Nomenclature of amphiboles: report of the Subcommittee on Amphiboles of the International Mineralogical Association, Commission on New Minerals and Mineral Names. *Can. Mineral*., **35**, 219-246.

Mongkoltip, P. & Ashworth, J.R. (1983): Exsolution of ilmenite and rutile in hornblende. *Am. Mineral*., **68**, 143-155.

Morrison, J. (1991): Compositional constraints on the incorporation of Cl into amphiboles. *Am. Mineral*., **76**, 1920-1930.

Popp, R.K. & Bryndzia, L.T. (1992): Statistical analyses of Fe^{3+}, Ti and OH in kaersutite from alkali igneous rocks and mafic mantle xenolits. *Am. Mineral*., **77**, 1250-1257.

Puga, E. (1990): The Betic Ophiolitic Association (south-eastern Spain). *Ofioliti*, **15**, 97-117.

Puga, E., Ruiz Cruz, M.D., Díaz de Federico, A. (1999): Magnetite-silicate inclusions in olivine of ophiolitic metagabbros from the Mulhacén Complex, Betic Cordillera, Southeastern Spain. *Can. Mineral*., **37**, 1191-1209.

Puga, E., Nieto, J.M., Díaz de Federico, A. (2000): contrasting P-T paths in eclogites of the Betic Ophiolitic Association, Mulhacén Complex, southeastern Spain. *Can. Mineral.*, **38**, 1137-1161.

Puga, E., Ruiz Cruz, M.D., Díaz de Federico, A. (2002): Polymetamorphic amphibole veins in metabasalts from the Betic Ophiolitic Association at Cóbdar, Southeastern Spain. Relics of ocean-floor metamorphism preserved through the Alpine orogeny. *Can. Mineral*., **40**, 67-83.

Puga, E., Fanning, M., Nieto, J.M., Díaz de Federico, A. (2005): Recrystallization textures in zircon generated by ocean-floor and eclogite-facies metamorphism: A cathodoluminiscence and U-Pb SHRIMP study, with constraints from REE elements. *Can. Mineral.* **43,** 183-202.

Raase, P. (1974): Al and Ti content of hornblende, indicators of pressure and temperature in regional metamorphism. *Contrib. Mineral. Petrol*. **45**, 231-236.

Robinson, P., Jaffe, H.W., Ross, M., Klein, C. (1971): Orientations of exsolution lamellae in clinopyroxenes and clinoamphiboles: Consideration of optimal phase boundaries. *Am. Mineral*., **56**, 909-939.

Robinson, P., Spear, F.S., Schumacher, J.C., Laird, J., Klein, C., Evans, B.W., Doolan, B.L. (1982): Phase relations of metamorphic amphiboles: Natural occurrence and theory. *Rev. Mineral*., **9B**, 1-227.

Schumacher, J.C. (1979): The estimation of the proportion of ferric iron in the electron-microprobe analysis of amphiboles. *Can. Mineral*., **35**, 238-246.

Shau, Y.-H., Peacor, D.R., Ghose, S., Phakey, P.P. (1993): Submicroscopic exsolutions in Mn-bearing alkali amphiboles from Tirodi, Maharashtra, India. *Am. Mineral*., **78**, 96-106.

Smelik, E.A. & Veblen, D.R. (1989): A five-amphibole assemblage from blueschists in northern Vermont. *Am. Mineral*., **74**, 960-965.

–, – (1991): Exsolution of cummingtonite from glaucophane: A new orientation for exsolution lamellae in clinoamphiboles. *Am. Mineral*., **76**, 1103-1118.

–, – (1992): Exsolution of Ca-amphibole from glaucophane and the miscibility gap between sodic and calcic amphiboles. *Contrib. Mineral. Petrol.,* **112,** 178-195.

–, – (1994): Complex exsolution in glaucophane from Tillotson Peak, North-central Vermont. *Can. Mineral*., **32**, 233-255.

Smelik, E.A., Nyman, M.W., Veblen, D.R. (1991): Pervasive exsolution within the calcic amphibole series: TEM evidence for a miscibility gap between actinolite and hornblende in natural samples. *Am. Mineral*., **76**, 1184-1204.

Thompson, J.B. (1982a): Composition space: an algebraic and geometric approach. *Rev. Mineral*., **10**, 1-32.

– (1982b): Reaction space: an algebraic and geometric approach. *Rev. Mineral*., **10**, 33-52.

Volfinger, M., Robert, J.-L., Vielzeuf, D., Nieva, A.M.R. (1985): Structural control of the chlorine content of OH-bearing silicates (micas and amphiboles). *Geochim. Cosmochim. Acta*, **49**, 37-48.

Zingg, A.J. (1996): Immiscibility in Ca-amphiboles. *J. Petrol*., **37**, 471-496.

Received 9 October 2006
Modified version received 23 February 2007
Accepted 7 May 2007